Journal of Hydrology 573 (2019) 123–135

Contents lists available at ScienceDirect

Journal of Hydrology

journal homepage: www.elsevier.com/locate/jhydrol

Research papers

Impacts of climate change on watershed systems and potential adaptation through BMPs in a drinking water source area

Jiali Qiu[a], Zhenyao Shen[a,*], Guoyong Leng[b], Hui Xie[a], Xiaoshu Hou[a], Guoyuan Wei[a]

[a] State Key Laboratory of Water Environment Simulation, School of Environment, Beijing Normal University, Beijing 100875, PR China
[b] Environmental Change Institute, University of Oxford, Oxford OX1 3QY, UK

ARTICLE INFO

This manuscript was handled by Emmanouil Anagnostou, Editor-in-Chief, with the assistance of Zoi Dokou, Associate Editor

Keywords:
Climate change
Nonpoint source pollution
BMP efficiency
BMP optimization
Miyun Reservoir Watershed

ABSTRACT

Climate change, in terms of changes in temperature and patterns of precipitation, has significant impacts on water resources and watershed ecosystems. Adapting to climate change is becoming an important strategy for watershed management. The goal of this study was to quantify the impacts of climate change on watershed hydrological processes and water quality, to evaluate the efficiency of Best Management Practices (BMPs) and the possible effects of a changing climate, and to configure cost-effective BMPs at sub-basin scale using a multi-objective optimization method to mitigate climate effects on water resource. The Soil and Water Assessment Tool (SWAT) model was used to simulate the possible effects of changing climate on watershed hydrological and water-quality processes and adaptation options in the Miyun Reservoir Watershed (MRW). Climate change had significant impacts on water balance components such as precipitation, runoff, and evapotranspiration (ET) and on water-quality components such as sediment and nutrient loads. A substantial decreasing trend of runoff indicated that the Miyun Reservoir faced a more acute challenge of insufficient water-supply capacity. Compared with baseline climate, climate change represented by precipitation and temperature regimes resulted in substantial increases in sediment load (12.95%) and nutrient losses (7.26% for TN and 9.56% for TP) on average all sub-basins. Climate variability had significant effects on BMP efficiency through effects on watershed hydrology, soil erosion, and nutrient losses. Results highlight the importance of optimal configuration of site-specific BMPs at sub-basin scale for adaptation to climate change. The methods and findings presented here hold promise to enhance the resilience of the watershed system to current and future climate change.

1. Introduction

In recent years, water resources at global scale have come under considerable stress from altered hydrological and diffused pollution conditions resulting from climate change. Changes in streamflow, water temperature, and water quality due to climate change will contribute to uncertainties in water supply and ecosystem health. The Miyun Reservoir Watershed (MRW) is the water protection area of the Miyun Reservoir, which supplies clean drinking water for a population of 21.75 million and is used to support rapid economic development in China's capital, Beijing. Diffused pollution from the upstream catchment by climate forcing such as precipitation and temperature, including soil erosion, nutrient releases from fields, casual wastewater discharges, and pollution washed out by rainfall and runoff, is the major threat to the water resources in the Miyun Reservoir because it potentially causes eutrophication (Lv et al., 2016). Water-supply shortages and gradual deterioration in water quality in the Miyun Reservoir have further threatened Beijing's drinking water security. Ma et al. (2010) reported that climate variability contributed to 55% of the decrease in inflow into the Miyun Reservoir during 1956–2005. The impacts of climate change on water quality in the Miyun Reservoir have been understudied.

The advent of climate change has affected precipitation patterns with regard to frequency, strength, spatial range, and duration, which will have substantial effects on hydrology and water quality, including surface runoff, soil erosion, and contaminant transport and deposition processes. Increased temperatures may affect the interactions among biological, physical, and chemical components and cause shifts in the timing of runoff peaks by changing the timing of snowmelt, especially in specific watersheds where precipitation is winter-dominant and stored in snowpack (Dudula and Randhir, 2016; Kim et al., 2015). Adapting to climate change is becoming an important concern or strategy to manage runoff and nonpoint source (NPS) pollution in watershed systems. The configuration of effective Best Management

* Corresponding author.
E-mail address: zyshen@bnu.edu.cn (Z. Shen).

https://doi.org/10.1016/j.jhydrol.2019.03.074
Received 9 January 2019; Received in revised form 18 March 2019; Accepted 21 March 2019
Available online 22 March 2019
0022-1694/ © 2019 Elsevier B.V. All rights reserved.

Practices (BMPs) at sub-basin level can help mitigate the impact of climate change on watershed hydrology and water quality. Climate change is involved in evaluating of hydrological and water-quality processes at catchment to regional scale and even the continental scale based on process-based models and statistical methods derived from long-term historical data (Sun et al., 2016). The Soil and Water Assessment Tool (SWAT) model is an integrated assessment tool that couples climate forcing, land-surface characteristics, and point source pollution inputs, which are important for representing watershed hydrological cycle and sediment, pesticide, nitrogen, and phosphorus transport processes at a variety of spatial and temporal scales (Arnold et al., 1998; Hashemi et al., 2016; Volk et al., 2017). Furthermore, the SWAT model has been proven effective for evaluating BMPs under complex terrains and varying climatic conditions in agriculture-dominant watersheds (Jayakody et al., 2014; Panagopoulos et al., 2015). This study used the SWAT model to assess the impacts of climate change on hydrology and water quality and evaluate the impacts of BMPs on developing adaptation strategies at sub-basin scale in the MRW.

BMPs can be implemented individually or designed as a management system, in which case individual practices are linked together or distributed as a spatial network, achieving complete control at source, field, path, watershed, and regional scales. These practices can also be used in mitigating and adapting to climate change by regulating climate, intercepting runoff, trapping sediment, and sequestering nutrients (Charlesworth, 2010). The negative impacts of climate change are strengthening, resulting in changes in hydrology, increasing pollutant loads, pressure on drinking water security, and a significant economic cost for revitalizing degraded environments. It is therefore imperative to understand and quantify the impacts of climate change to develop an effective management plan for water resources (Kiedrzynska et al., 2015; Saraswat et al., 2016; Valcu-Lisman et al., 2017). A number of approaches are provided to develop sustainable watershed management systems accounting for both environmental and economic benefits (Haas et al., 2017; Liu et al., 2017; Valcu-Lisman et al., 2017). The simulation-optimization framework proposed by Qiu et al. (2018) serves as a multi-objective optimization tool based on the Non-dominated Sorting Genetic Algorithm II (NSGA-II) for exploring tradeoffs among economic costs, water-quality improvements, and decision-makers' concerns regarding BMP design by coordination across sub-watersheds. NSGA-II is often used to optimize BMP selection and placement at watershed scale due to its global optimization ability to address multi-objective and high-dimensional problems with the crowded comparison operator and to find true Pareto-optimal solutions with a limited number of simulation runs (Deb et al., 2002). This framework used the NSGA-II expanded with an auto-adaptive control parameter adjustment algorithm to generate spatial BMP configurations at sub-basin scale. Hence, this approach was used here to explore optimal BMPs considering water-quality responses to climate change.

The future climate change scenarios were driven by multiple Representative Concentration Pathways (RCPs) that depend on specific greenhouse gas concentrations to reach a particular radiative forcing in the year 2100. Future climate variability can be predicted by general circulation models (GCMs) based on RCP scenarios, the outputs of which should be downscaled and bias-corrected across a dense grid overlaid on the study area. The bias-correction algorithm with spatial disaggregation helps correct the future climate data by the transfer factors constructed between GCMs and actual historical observations (Hempel et al., 2013; Leng and Tang, 2014). The future time series of climate variables are added into the watershed models (e.g., SWAT) to evaluate long-term changes in surface runoff, streamflow and water quality.

To develop adaptation strategies for the climate variability that are site-specific to sub-basins, this paper evaluates the impacts of climate change on hydrology and water quality and the efficiency of BMPs in mitigating these impacts in an agriculture-dominated watershed. Specifically, the MRW will be taken as the study area to explore potential adaptation strategies through BMP configurations at sub-basin scale in near, middle, and far future periods. The objectives of the study are to 1) simulate hydrological and water-quality processes using a SWAT-based watershed model calibrated by current climate forcing, land use, soil types, topography, water quality, and crop management data; 2) evaluate the impacts of climate change on the water balance and on pollutant losses in three future periods compared to the simulated results under the baseline climate; 3) evaluate the impacts of climate change on BMP efficiency compared with the simulated results for baseline climate; 4) investigate adaptation strategies by optimizing BMP placement at sub-basin scale to help reduce the impacts of climate change. Results were evaluated in terms of changes in surface runoff, actual evapotranspiration (ET), potential evapotranspiration (PET), sediment yields, and nutrient losses.

2. Materials and methods

2.1. Watershed description

The MRW (40°19′-41°36′N and 115°27′-117°35′E) is located across Beijing and Hebei Province. It consists of two sub-watersheds: the Chao River sub-watershed and the Bai River sub-watershed, which are the upstream catchments of the Miyun Reservoir and cover an area of 5892.97 km^2 and 9030.98 km^2 respectively. The Miyun Reservoir is the largest reservoir in northern China and the most important potable water source for Beijing. Many studies have stated that climate variations contributed to large decreases in runoff in the historical period and seriously affected Beijing's water supply (Ma et al., 2010; Zheng et al., 2016). Changes in hydrology strongly influence water-quality processes in a watershed system, especially NPS pollution driven by precipitation and runoff (Geng et al., 2015).

Geographical information, including topography, land use, and soil type, was used to set up the SWAT model. Topographic data were represented by a 90 m spatial resolution digital elevation model (DEM) obtained from the National Geomatics Center of China. Land-use data referred to a 1:100,000 digital land-use map (Fig. S1 in the in the Supplementary Material) obtained from the Institute of Geographical and Natural Resources Research, Chinese Academy of Sciences. Soil type information was extracted from a 1:1,000,000 digital soil map of China, which was provided by the FAO Harmonized World Soil Database. Soil properties were obtained from the Soil Research Institute of the Chinese Academy of Sciences or calculated by the SPAW (Soil-Plant-Air-Water) model (Saxton and Rawls, 2006). Historic hydrological and water-quality data from the survey stations located at the outlets of the two upstream sub-watersheds were used to develop a calibrated model. Observed daily weather data were provided by gauges scattered throughout the watershed. Future climate variability projections separately generated by five GCMs were used to assess climate effects for the period 2020–2099. Table S1 in the Supplementary Material gives a description of the database for the SWAT setup.

2.2. Model description

The SWAT model was developed by the USDA Agricultural Research Service (USDA-ARS) and Texas A&M University and is continuously upgraded with interfaces in combination with ArcGIS (Arnold et al., 2012a). It is a process-based model that simulates water quantity and pollutant transport and predicts the impacts of land-surface characteristics, climate change, and management practices at watershed scale (Arnold et al., 1998). In the SWAT model, a watershed is divided into multiple sub-basins based on topographic information, and sub-basins are further subdivided into small units called hydrologic response units (HRUs), which are homogeneous areas processing unique land cover, soil type, slope, and landscape characteristics for simulations of the hydrological cycle and pollutant transport through the land phase and

the channel network (Arnold et al., 2012a). In this study, the SWAT model was calibrated and validated with observed historical climate data for periods of 1990–1998 and 1999–2010 respectively. More details of parameter sensitivity (Tables S2 and S3) and model calibration and validation were given in the Supplementary Material. Following calibration, the baseline (1980–2004) and future climate data (2020–2099) from the five GCMs were input into the model to identify the impacts of climate change on water balance, water quality and BMP efficiency in the MRW and to avoid the potential bias that was caused by running a present-day model with future climate inputs driven by the downscaled GCMs. SWAT accounts for a wide array of land, nutrient, and structural management practices to assess the efficiencies of BMPs in controlling the amount of runoff and pollutant losses entering channels in watersheds by calculating changes in water quantity and quality with and without BMP (Waidler et al., 2011). Table S4 in the Supplementary Material shows the modules and key parameters for BMP assessment.

2.3. Climate change scenarios

Bias-corrected future climate data at daily time step, including precipitation, air temperature (maximum and minimum), solar radiation, wind speed, and relative humidity, were provided at 0.5 × 0.5 spatial resolution from five GCMs (GFDL-ESM2M, HadGEM2-ES, IPSLCM5A-LR, MIROC-ESM-CHEM, and NorESM1-M) that are recommended in the framework of the Inter-Sectoral Impact Model Intercomparison Project (ISI-MIP) (Table S5 in Supplementary material). The GCMs were driven by the four representative concentration pathway (RCP) scenarios: RCP 2.6 (very low greenhouse gas concentrations) (van Vuuren et al., 2007), RCP 4.5 (medium low greenhouse gas concentrations) (Smith and Wigley, 2006), RCP 6.0 (medium high greenhouse gas concentrations) (Hijioka et al., 2008), and RCP 8.5 (high greenhouse gas concentrations) (Riahi et al., 2007). A distribution-based bias-correction algorithm was used to correct the climate data from GCMs, which were used to ensure that GCM data matched the climatology of the WFD (Water and Global Change (WATCH) Forcing Data) over the reference period of 1960–1999 (Leng and Tang, 2014). In this method, the derived correction factors linearly regressed between GCM and WFD were used to correct the projected GCM data for future periods. Details of the bias-correction algorithm are given in Hempel et al. (2013).

The RCPs are consistent with certain socio-economic assumptions and possible changes in future greenhouse gas emissions from anthropogenic activities and aim to represent the atmospheric concentrations that drive possible changes in temperature and precipitation in future periods (van Vuuren et al., 2011). RCP 2.6 assumes that the concentrations peak during 2010–2020 and then substantially decline, which contributes to the lowest possibility of climate change. RCP 4.5 assumes that greenhouse gases peak around 2040, then decline, which contributes to a low possibility of climate change. RCP 6.0 assumes that the concentrations peak around 2080, then decline; this process contributes to a large possibility of climate change. RCP 8.5 assumes that greenhouse gas concentrations continue to rise throughout the 21st century; this scenario exhibits the highest levels of forcing and the largest possibility of climate change. This study focused on climate variability driven by RCP 8.5 to assess the impacts of climate change on hydrology and water quality in the MRW.

2.4. BMP optimization method

This study used a BMP optimization approach to determine potential BMP configurations at sub-basin scale to achieve the water-quality improvement targets at the minimum economic cost. Details of this approach are available in Qiu et al. (2018), which proposed a systematic optimization framework combining a watershed model (SWAT model), an economic module (Farm-level Economic model (FEM)), a Markov Chain method, and a modified Non-dominated Sorting Genetic Algorithm II (NSGA-II). The SWAT model was used to evaluate the pollution reduction effects of candidate BMPs. The FEM was used to evaluate the economic costs of BMPs, including construction cost, maintenance cost, and economic benefits. The NSGA-II algorithm expanded with an auto-adaptive control parameter adjustment method (Chen et al., 2015) was used to generate Pareto-optimal spatial BMP configurations to ensure that water-quality improvement targets were met at multiple assessment points through coordinated optimization of the two upstream sub-watersheds. The Markov Chain method was used to calculate pollutant loads at the assessment points with various BMP configurations or no BMP scenario based on upstream and downstream information about the watershed (Chen et al., 2016). Fig. S2 in the Supplementary Material illustrates this simulation-optimization framework.

3. Results and discussion

3.1. Future climate variability

The nonparametric Mann-Kendall (MK) test (Kendall, 1975; Mann, 1945) was used to determine the significance of trends in mean annual precipitation (PREC), annual rainfall days in different rain patterns, annual maximum temperature (T_{max}), minimum temperature (T_{min}), and mean temperature (T) from 2020 to 2099. Table 1 shows the long-term annual trend test results at the 5% significance level evaluated by the MK test from the time series of climate variables in the MRW that were predicted by the five GCMs. There was an uptrend in annual precipitation under RCP 2.6, RCP 4.5, RCP 6.0 scenarios, but not a significant one, with mean annual change of 0.732, 0.625 and 0.602 mm/year respectively, and a significant upward trend with 0.881 mm/year for RCP 8.5, which can be attributed to the increase in the frequency of rainfall events, especially extremes such as heavy rain and rainstorms. The mean changes in annual days of heavy rain were 0.039, 0.036, 0.039 and 0.047 days/year for RCP 2.6, RCP 4.5, RCP 6.0, and RCP 8.5 respectively, and the mean changes of rainstorm events were 0.011, 0.011, 0.014 and 0.019 days/year for these four RCP scenarios respectively, which indicated an uptrend in the frequencies of heavy rain and rainstorm events. These results were consistent with other applications in similar regions (Pan et al., 2016). A remarkable increase in frequency of rainstorm and heavy rain events would cause increased soil erosion and water quality problems in the future. (Fig. 1)

As shown in Table 1 and Fig. 2, monthly temperatures significantly increased in all future scenarios compared with the baseline period, and RCP 8.5 led to a most remarkable increase due to the highest greenhouse gas concentrations. July and August were the warmest months in the baseline period, but in future climate, the warmest months will extend over a long period from June to September. As shown in Fig. 3, a substantial increase in the rate of change of T_{min} prompted a substantial increase in average temperature in RCP 8.5, and the amounts of precipitation showed a critical increasing trend. Significant variations in precipitation and temperature driven by RCP 8.5 scenario will have substantial impacts on watershed hydrology and pollutant transport and transformation processes through soil erosion, runoff, and washoff. Therefore, this study focused on the impacts of climate change driven

Table 1
Trends in mean annual precipitation (mm/year) and temperature (°C/year) for the period of 2020–2099 detected by MK test.

Variable	RCP 2.6	RCP 4.5	RCP 6.0	RCP 8.5
Annual precipitation (mm/year)	0.732	0.625	0.602	0.881*
Annual T_{max} (°C/year)	0.016	0.009	0.006	0.081*
Annual T_{min} (°C/year)	0	0.004	0.039*	0.071*
Annual mean temperature (°C/year)	0.007*	0.028*	0.040*	0.069*

* Significant trends at 5% significance level of two-tailed tests.

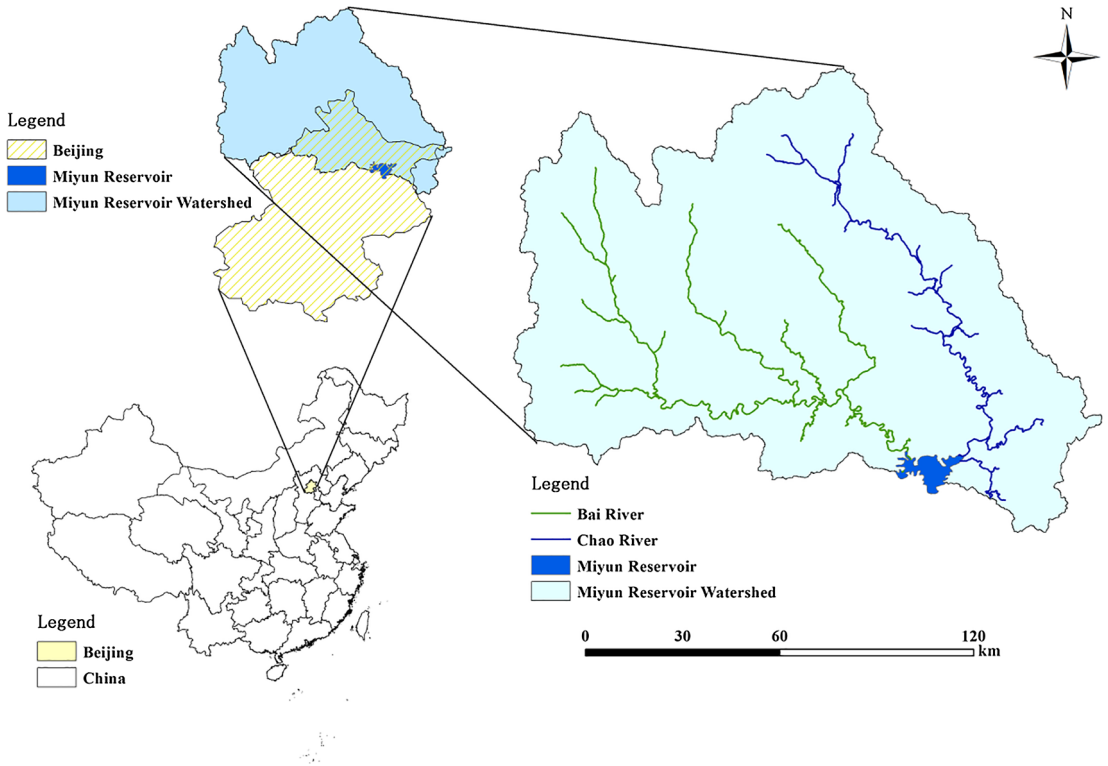

Fig. 1. Location of the Miyun Reservoir Watershed.

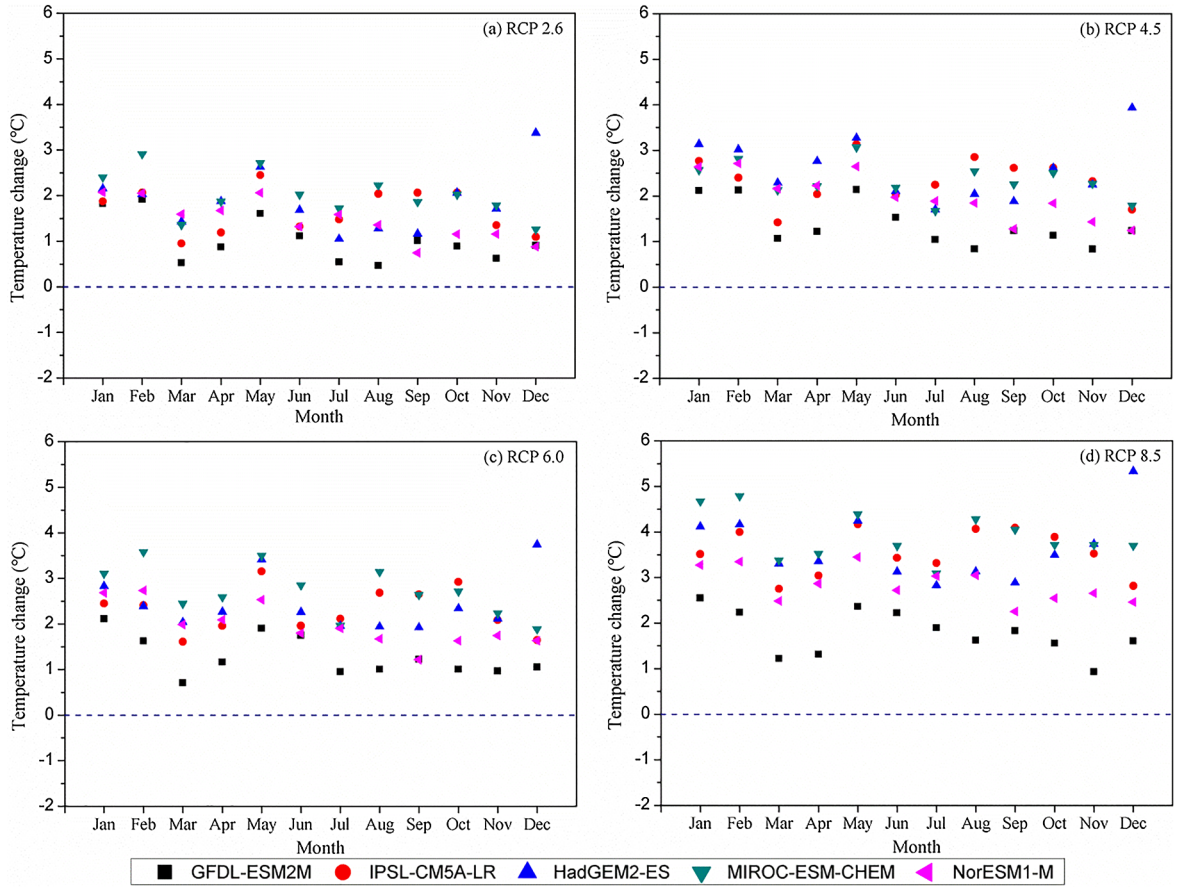

Fig. 2. Projected changes in average monthly temperature by 5 GCMs for four RCP scenarios: (a) RCP 2.6, (b) RCP 4.5, (c) RCP 6.0, and (d) RCP 8.5.

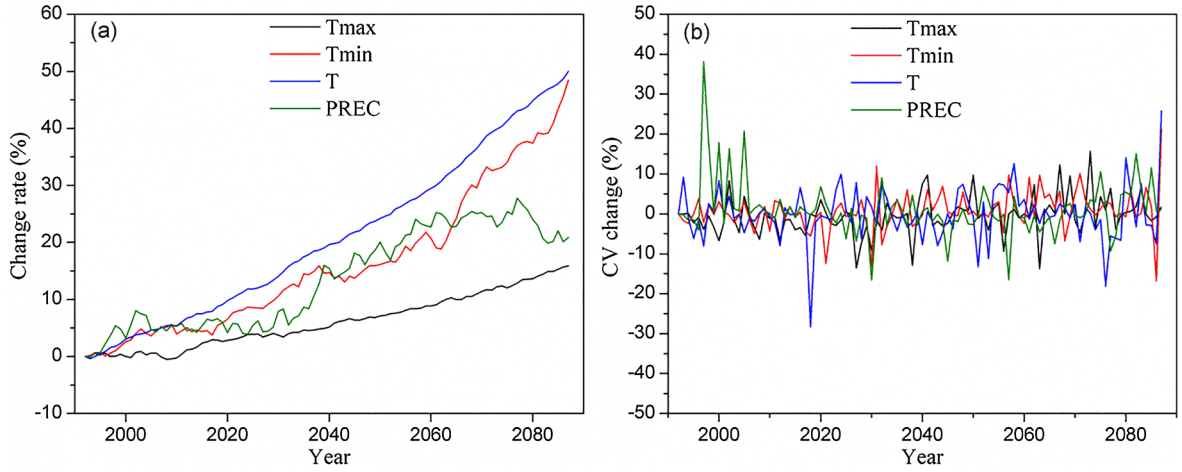

Fig. 3. Ensemble average percentage changes in (a) annual mean precipitation (*PREC*), mean temperature (*T*), maximum temperature (T_{max}), and minimum temperature (T_{min}); (b) their CVs throughout 2020–2099 under the RCP 8.5 scenario. The changes are calculated for each 25 years running average in the time series with respect to the baseline period of 1980–2004.

by RCP 8.5.

3.2. Water balance under the impacts of climate variability

The calibration and validation of monthly hydrological and pollutant simulations were evaluated by the coefficient of determination (R^2) and the Nash-Sutcliffe efficiency (*Ens*), which are listed in Table 2. The majority of the statistics satisfied the judging criteria for model performance, although sediment results were distinctly weaker, mainly affected by the paucity of observed sediment data and the shorter simulation periods for both calibration (2006–2008) and validation (2009–2010). These results indicate that SWAT could accurately simulate the hydrology and contaminants in the MRW.

The calibrated SWAT model was used to simulate the water balance under the various climate change scenarios. Table 3 shows mean annual simulated water balance components integrated from all the simulated results based on future climate data from the five GCMs. On average, annual precipitation in future climate ranged from a minimum of 582.44 mm to a maximum of 701.97 mm. This corresponds to changes of 3.64–24.91% relative to baseline climate. Precipitation increased during the colder period of the year (Fig. 4), which was clearly caused by a consistent increase in temperature across all the GCMs given the fact that precipitation increased in all the cold months when snowfall can occur. This contributed to a reduction in snowfall within the cold period of the year. Table 3 implies substantial increases in ET and PET, with changes of 9.74% and 3.02%. This result occurred because all the GCMs predicted high temperature and net radiation increases in future periods, which have a direct impact on ET and PET in the MRW.

Table 2
Monthly calibration and validation statistical results.

Variable	Indices	Chao River		Bai River	
		Calibration	Validation	Calibration	Validation
Flow (m^3/s)	R^2	0.876	0.722	0.635	0.541
	Ens	0.836	0.503	0.591	0.486
Sediment (ton)	R^2	0.750	0.627	0.750	0.633
	Ens	0.424	0.394	0.738	0.601
TN (kg)	R^2	0.731	0.628	0.592	0.620
	Ens	0.531	0.487	0.525	0.441
TP (kg)	R^2	0.812	0.773	0.634	0.528
	Ens	0.788	0.528	0.528	0.497

Table 3
Mean annual water balance components in the MRW for the baseline period of 1980–2004 or for future period of 2020–2099 under the five GCMs.

Climate Scenario	Water balance indicators (mm)				
	Precipitation	Surface runoff	Total water yield	ET	PET
Baseline climate	561.97	84.69	229.99	316.72	1024.17
GFDL-ESM2M	625.06	58.43	227.58	332.51	1007.72
HadGEM2-ES	701.97	138.01	325.72	357.48	1087.92
IPSL-CM5A-LR	666.22	59.34	226.92	361.42	1096.22
MIROC-ESM-CHEM	582.44	30.46	168.44	345.65	1046.24
NorESM1-M	605.02	35.88	180.60	340.84	1037.13
Average of all GCMs	636.25	68.12	225.79	347.58	1055.05
% change	13.22	−19.56	−1.83	9.74	3.02

The greater increase in ET (Fig. 4) in winter and spring was primarily driven by the significantly increased temperature during this period, which was consistent with the great increase in T_{min} noted in Section 3.1, yielding large changes in annual ET. The small ET increase in summer and autumn compared to spring and winter is also worth noting. This can be explained by the observation that almost all GCMs predicted greater temperature increases within the cooler part of the year, with direct impact on snowfall, but lesser temperature increases in the warmer part of the year, which in combination do not result in considerably altered ET values in this period; these results were consistent with other studies (Panagopoulos et al., 2015). On the other hand, the small increase in ET can also be attributed to the small increase in precipitation (water inputs) within the warmer period rather than to increased temperatures.

Mean annual runoff in different sub-basins predicted by the GCMs manifested a greater deviation compared to the baseline climate, ranging from a 53.48% decrease to a 55.36% increase in the sub-basins (Fig. 5). Runoff decreased by 18.83% on average in all sub-basins under the future climate, with average change rates of −30.14%, −22.17%, and −3.97% in the near, middle, and far future periods respectively, which was inconsistent with the increase of precipitation, although runoff tended to rise throughout the future period along with the continued increase of precipitation. This shows that runoff production is driven not only by water inputs into the basin following the precipitation predicted by different GCMs, but also by other hydrological factors such as the frequencies of different rain patterns throughout the year (Gao et al., 2018), rainfall intensity (Aguilar et al., 2016), ET

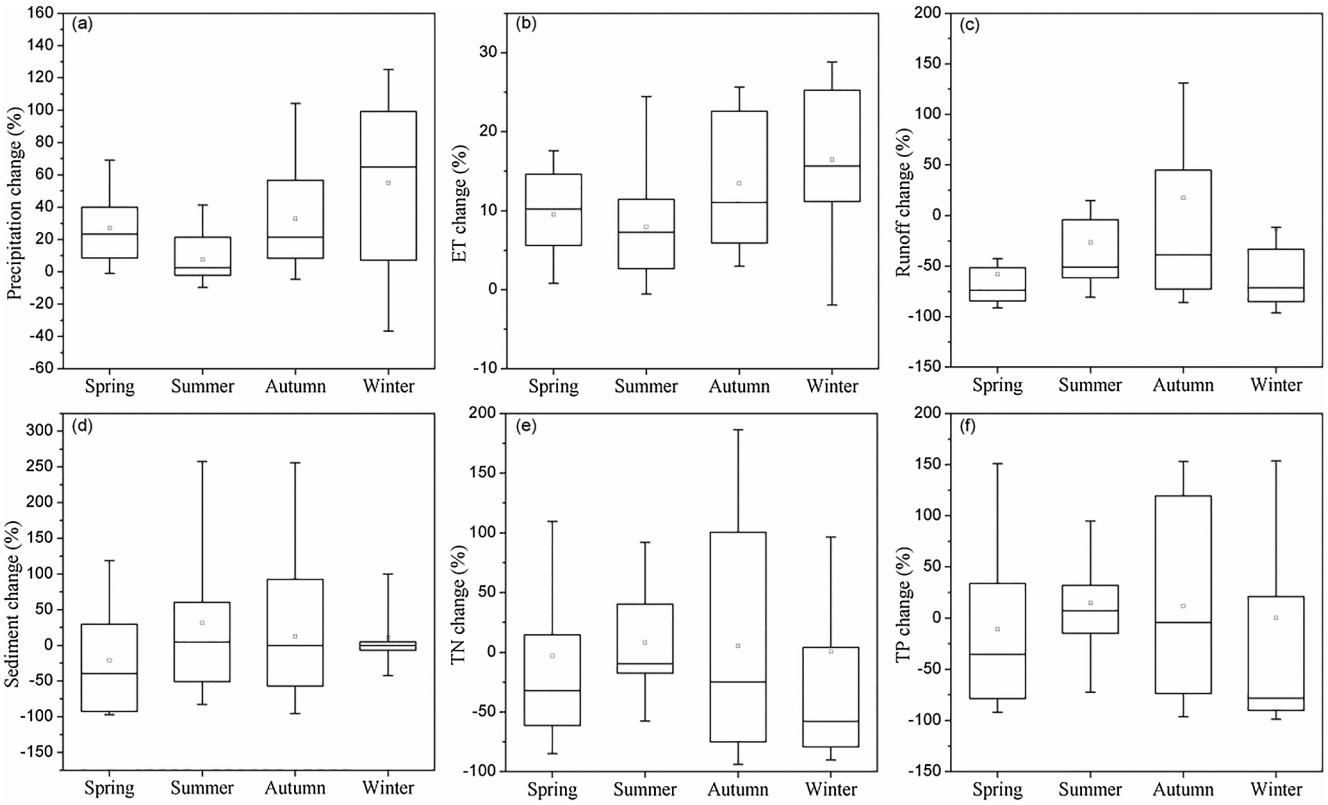

Fig. 4. Seasonal change rates of precipitation (a), evapotranspiration (b), runoff (c), sediment (d), TN (e), and TP (f) loads on sub-basins from the baseline climate for 2020–2099 under the five GCMs.

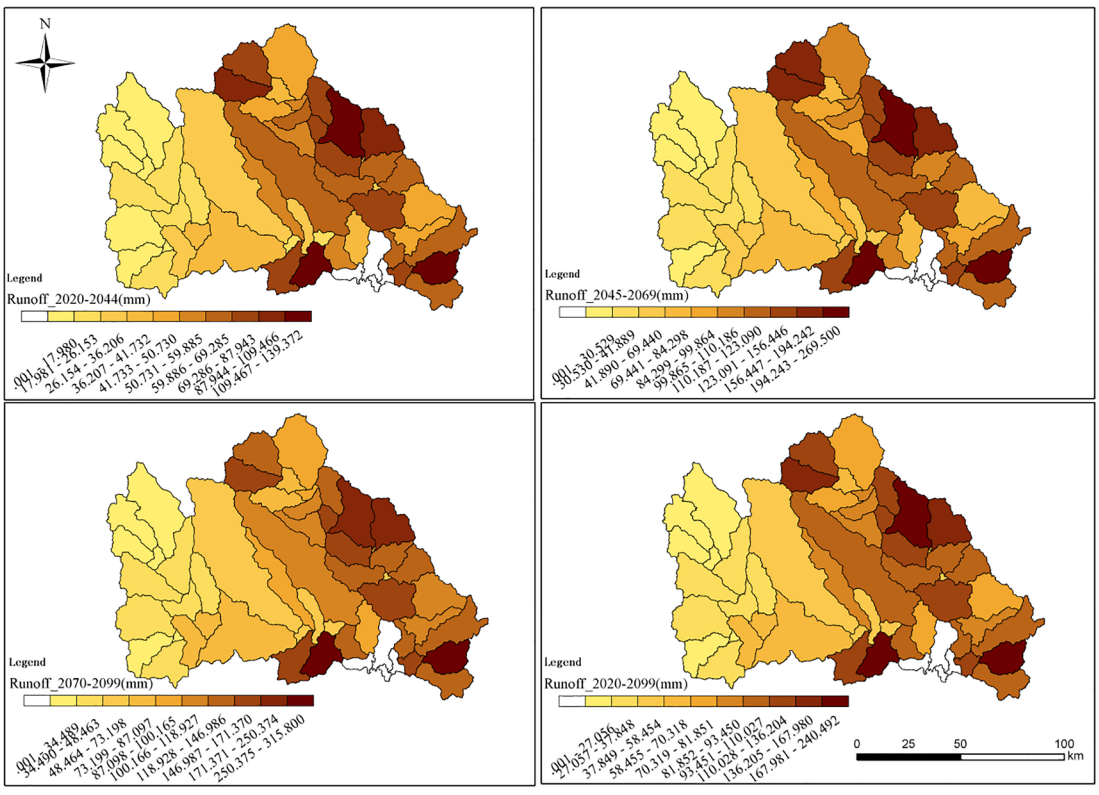

Fig. 5. Spatial distributions of average annual runoff in the near, middle and far future periods (RCP 8.5).

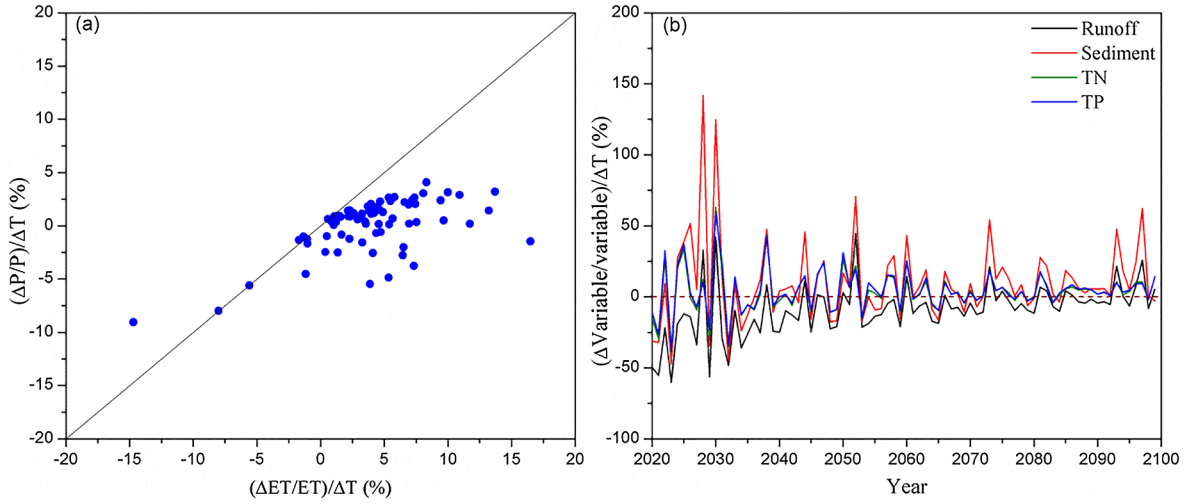

Fig. 6. Relationship between changes in precipitation and ET under unit temperature increase (a), and changes in runoff, sediment yields, TN and TP loads under unit temperature increase (b) related to baseline climate (1980–2004).

amount (Milly and Dunne, 2016), soil properties (infiltration rate) (Grillakis et al., 2016), and surface characteristics (Sofia et al., 2019). This study analyzed changes in water balance components to explain the decrease in runoff. The decrease in generated runoff during June-September was driven by a small increase in precipitation and a relatively large increase in ET, which was caused by a consistent increase in temperature across the future periods predicted by all GCMs. Fig. 6(a) shows a substantial mean increase of 4.10% in ET under unit increasing temperature, but a small increase of 1.79% in precipitation volume. Increasing water input less than water loss was bound to cause a decrease of 9.01% in runoff yields for a unit increase in temperature (Fig. 6(a)). This result further implied that climate warming plays a crucial role in significantly reducing streamflow (Zheng et al., 2016). The substantially higher temperatures in the coldest months contributed to more precipitation falling as rain than as snow; this result caused a small decrease in runoff in winter. However, the low frequency of snowfall caused snowmelt runoff in spring to decrease, which was characterized as a substantial decrease in runoff (Fig. 4). In addition, reductions in water yield were likely exacerbated by increased water consumption for domestic and industrial uses in this watershed (Zheng et al., 2016). A significant decreasing streamflow trend indicated that the Miyun Reservoir would face further challenges of insufficient water-supply capacity to meet water demands for the ecosystem, agriculture, and domestic and industrial use. The change trends implied that climate change must be considered in watershed management strategies to ensure sufficient water-supply capacity of the Miyun Reservoir to meet increasing future water demands.

Generally, the spatial distribution of runoff (Fig. 5) was in agreement with the spatial distributions of land uses (Fig. S1 in the Supplementary Material). Forestland in the upstream sub-basins had an important function in water conservation and effectively reduced runoff due to the high vegetation coverage, and the areas with high runoff were concentrated in the downstream sub-basins where land uses were dominated by cropland, with poor water retaining capacity due to frequent agricultural activities and low vegetation coverage.

3.3. Pollutant losses under impacts of climate variability

The calibrated SWAT model was used to evaluate pollutant losses under the baseline climate in GCM reference period of 1980–2004. Sediment losses ranged from 0.69 to 199.26 t/ha and came mainly from agricultural land. TN and TP losses in the baseline period were predicted to range from 1.23 to 24.04 kg/ha and from 0.08 to 6.88 kg/ha respectively. The sediment and nutrient losses were higher in the sub-basins where agricultural land accounted for a large area. The contributions of different land covers were ranked as follows: cropland > barren land > pastureland > forestland > residential areas. Fig. S4 in the Supplementary Material shows the spatial distributions of pollution loadings in the baseline climate.

Fig. 7 shows the distribution of mean annual sediment yields in the MRW for the predicted climates. Compared to the results for the baseline climate, the mean annual rates of change at sub-basin scale were −10.41%, 4.73%, and 44.52% in the near, middle, and far future periods respectively. Sediment loads at sub-basin scale were significantly increased by 12.95% under future climate variability. Compared to the distribution of land cover (Fig. S1 in the Supplementary Material), the areas with high load intensity were distributed in the sub-basins with large areas of agricultural land, where soil erosion was prone to occur due to low vegetation coverage and increased frequency of heavy rain and rainstorms in future periods. This result played an important role in the spatial configuration of BMP.

The spatial distribution of sediment load intensity was similar to that of precipitation (Fig. S3 in the Supplementary Material) in the three periods. Although runoff shows a downward trend and has substantial effects on the decrease of sediment load in the near future period, the increasing trend of sediment load is consistent with that of precipitation (coefficient of determination $R^2 = 0.605$), which indicates that swift erosion of topsoil by rain was the main reason for the aggravation of soil erosion in future periods. The impact of millions of raindrops directly hitting the bare soil surface can be incredibly strong as they dislodge and splash soil particles into runoff and streams. This finding is similar to other future predictions that reported that increasing precipitation amount and intensity would increase sediment load in the future (Kim et al., 2015; Yasarer et al., 2017). On the other hand, it cannot be ignored that temperature has a strong influence on sediment yields and nutrient losses by altering soil parameters such as soil water content and soil temperature (Klik and Eitzinger, 2010). In this study, a unit increase in temperature was found to lead to a 10.11% increase in sediment load in the future period (Fig. 6(b)).

Figs. 8 and 9 present the mean annual TN and TP losses to waters for the various sub-basins. The results indicated that the spatial distributions of nutrient loads in the three future periods were consistent with those in the baseline period (Fig. S4), which were determined by surface characteristics (land covers, soil properties, and the watershed hydrodynamic network) in combination with agricultural activities and land management practices. The highly polluted sub-basins were dominated by cropland and barren land related to lower vegetation coverage, high soil disturbance intensity, and extensive application of

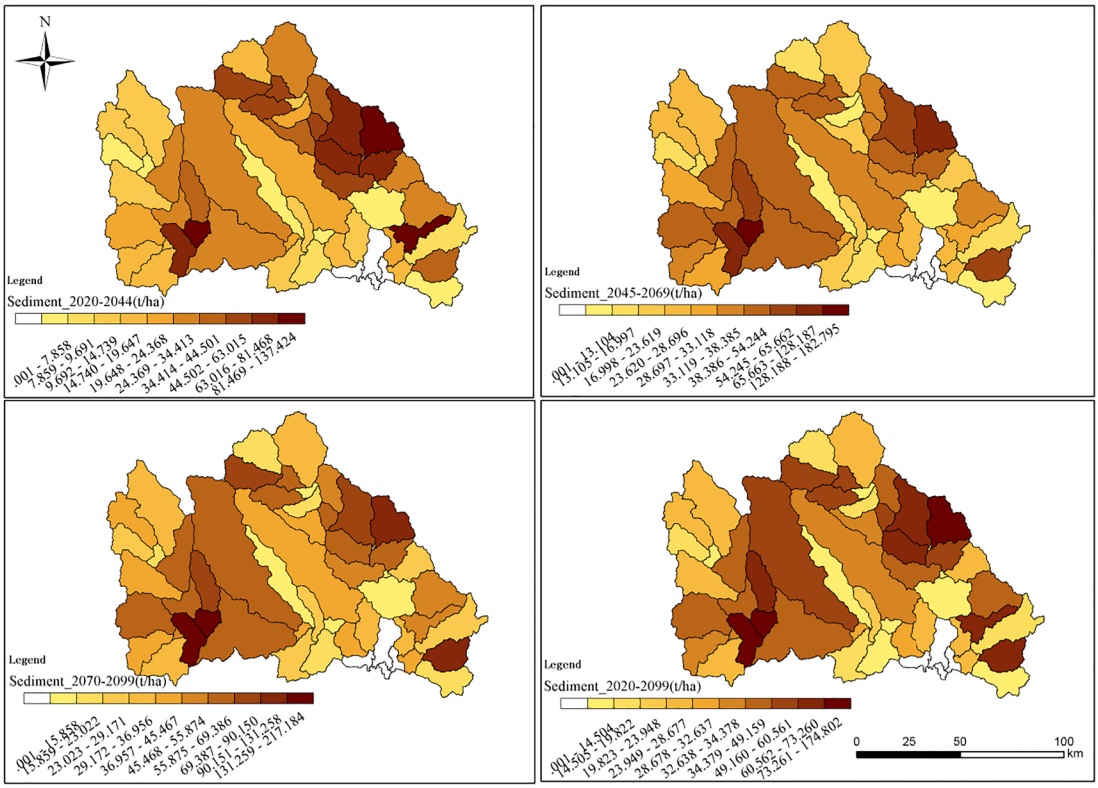

Fig. 7. Spatial distribution of average annual sediment load in the near, middle and far future periods (RCP 8.5).

fertilizers and manures. These results determined the spatial variation of BMP configuration. The mean change rates of annual TN and TP load intensities for all sub-basins were 6.52% and 5.67% respectively in the near future, 11.63% and 16.82% respectively in the middle future, and 3.63% and 6.19% in the far future. Their mean rates of change over the entire future period were 7.26% and 9.56% respectively. The distributions of nutrient load intensities were similar to those of sediment yields, which indicates that nutrient losses are closely related to soil

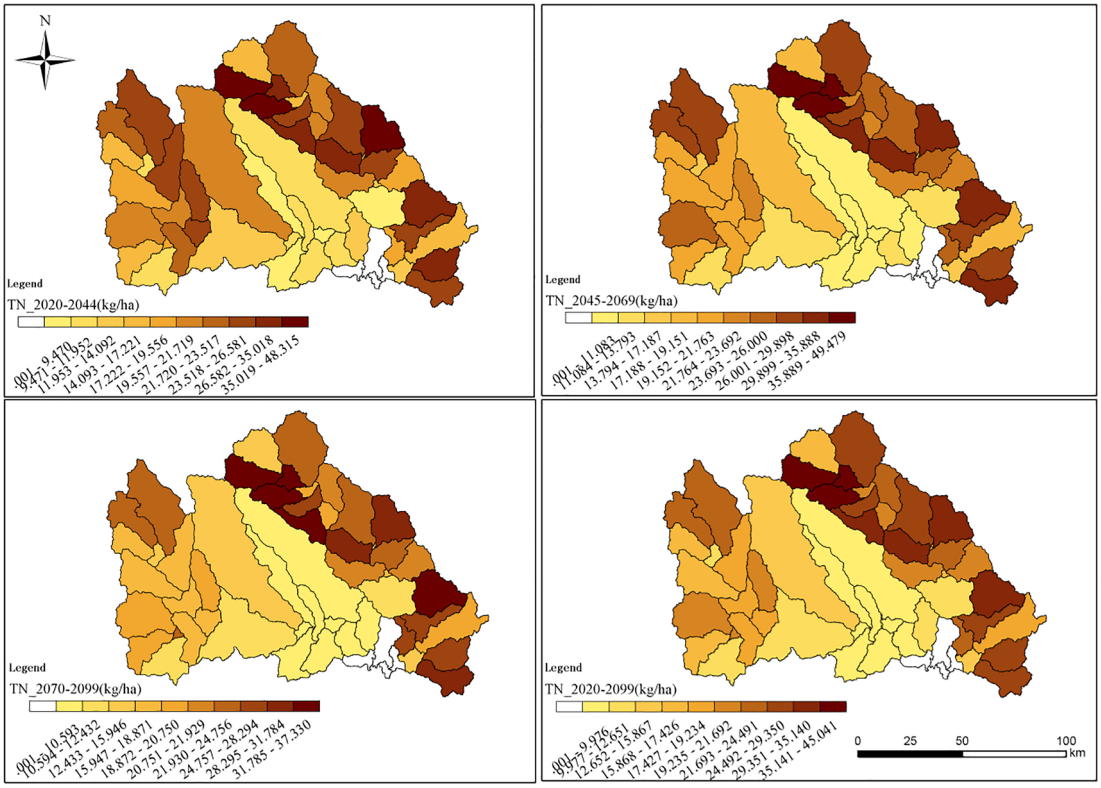

Fig. 8. Spatial distribution of average annual TN load in the near, middle and far future periods (RCP 8.5).

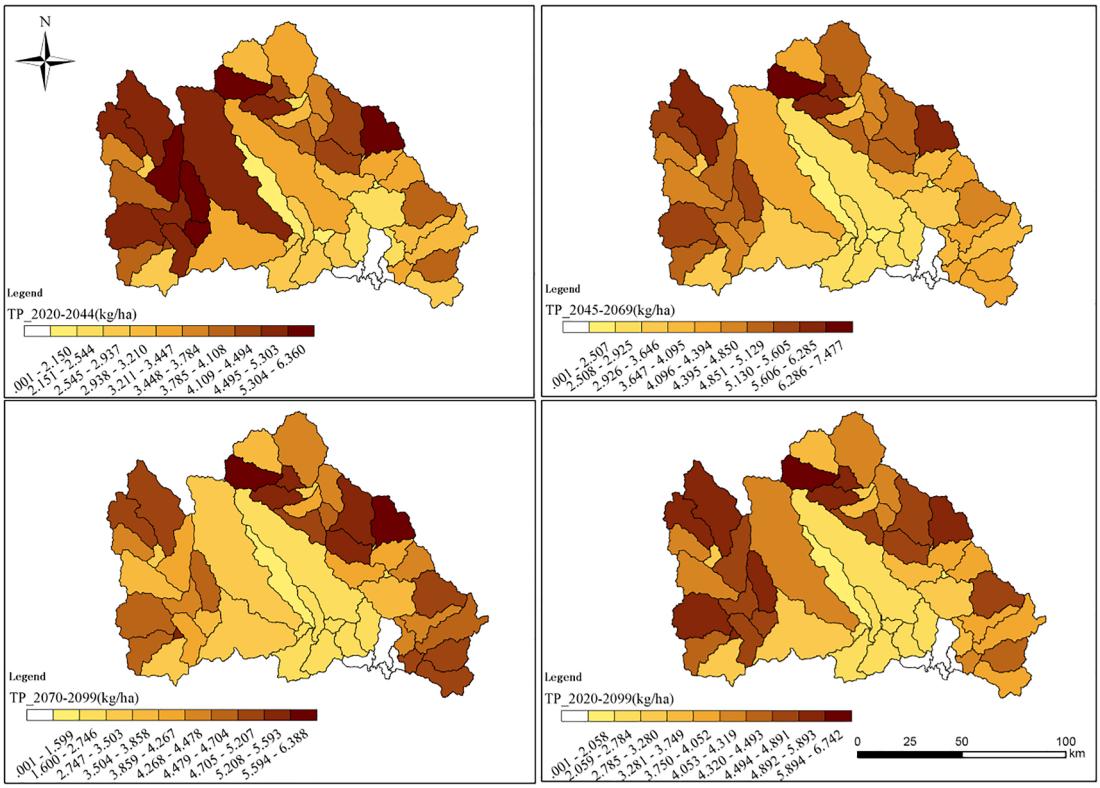

Fig. 9. Spatial distribution of average annual TP load in the near, middle and far future periods (RCP 8.5).

degradation, with nutrients either adsorbed on soil particles or in the soluble form (Comino et al., 2016). In this study, the coefficients of determination (R^2) between precipitation volumes and TN and TP loads were 0.704 and 0.657 respectively, which indicates that the effects of precipitation amount on nutrient losses are strong, but that they are not the only influencing factor for nutrient loads. The frequency of extremely dry and wet events will increase in the future, which may be another factor that increases the decomposition and flushing of organic matter and pollutants to surface runoff and may lead to increased nutrient loads in streams (Jayakody et al., 2014). High-intensity rainfall after a long dry period will increase pollutant loads into streams as the "first flush" occurs after long-term accumulation. This process will lead to immediate high concentrations of pollutants in surface water. Generally, climate change represented by increasing precipitation (volume and intensity) and increasing temperature will lead to higher sediment yield and more nutrient losses into surface runoff. Because high-intensity rainfall and extremely high temperatures will primarily occur in summer, TN and TP loads will significantly increase during this period (Fig. 4). The increase in temperature due to climate change will contribute to nutrient transformation among different forms, especially the mineralization processes that are directly related to soil temperature and the nutrient releases related to organic matter transport. In this study, TN and TP loads increased by 3.77% and 4.51% for each unit increase in temperature (Fig. 6(b)). This illustrates that changes in nutrient loads not only depend critically on precipitation, but also significantly on changes in temperature in the MRW. This result was supported by other studies (Kim et al., 2015; Klik and Eitzinger, 2010; Panagopoulos et al., 2015). Under warmer and wetter conditions, plant and microbial biomass utilize dissolved nutrients rapidly, which coupled with reduced mineralization and nitrification from fresh organic nutrient (Dudula and Randhir, 2016; Zessner et al., 2017), whereas organic nutrients were the main pattern of nutrient losses in the MRW. Rainfall instead of snowfall will be the main form of precipitation in winter as temperature increases, which will contribute to an increase in runoff and then lead to an increase in nutrient loads in winter, although nutrient concentrations will remain stable compared to the baseline period.

3.4. Impacts of climate change on BMP efficiency

Because watershed hydrology and water quality will be impacted by climate variability, future climate change must be a factor in designing watershed management strategies to protect water quantity and quality in the Miyun Reservoir to meet the increasing water-supply demands of Beijing. Quantifying the influence of climate change on BMP performance is important for managing water resources and developing cost-effective BMP scenarios to mitigate the impacts of climate change on water quality in the future. On the basis of local surface and pollution characteristics, stakeholders' preferences for BMPs, and socio-economic conditions, we selected several potentially feasible watershed management practices to evaluate their efficiencies in reducing sediment and nutrient loads under future climate conditions, including land management practices such as conservation tillage (CT), residue management (RM), converting farmland to forestland over slopes of 15° and 25° (CFF15 and CFF25), contour farming (CF), strip cropping (AC), nutrient management practices such as reducing fertilizer use by 20% and 30% (FR20% and FR30%), and structural BMPs such as filter strips with widths of 5 m, 10 m, and 15 m (FS5m, FS10m, and FS15m), grassed waterways (GW), constructed wetlands (CW), and detention basins (DB).

BMP efficiency was simulated using the BMP representation tool or module in the calibrated SWAT model (Arnold et al., 2012b; Renkenberger et al., 2017). As shown in Fig. S6 in the Supplementary Material and Table 4, the efficiency of each BMP varied over a wide range depending on climatic conditions. Compared to the results for baseline climate (Fig. S5 in the Supplementary Material), BMP efficiencies tended to decrease under climate variability, especially those of structural BMPs because these practices control water-quality components by intercepting runoff, which will decrease in the future. A filter strip is a vegetated strip established in the vicinity of farmland or

Table 4
Effectiveness of BMPs to reduce sediment and nutrient loads in the MRW.

BMP	% Change in sediment (t/ha)				% Change in TN (kg/ha)				% Change in TP (kg/ha)			
	Baseline	Near period	Middle period	Far period	Baseline	Near period	Middle period	Far period	Baseline	Near period	Middle period	Far period
CFF15	14.68	14.42	15.01	12.76	7.91	8.17	7.62	7.94	7.32	7.18	8.21	6.15
CFF25	11.19	11.32	11.77	10.02	7.66	7.29	7.46	7.12	7.23	6.70	7.11	6.29
FR20%	1.05	1.07	1.02	0.92	14.46	12.89	13.87	14.85	13.64	14.66	14.23	13.80
FR30%	1.46	1.12	1.07	0.97	14.99	14.65	14.33	14.01	14.16	15.02	14.68	14.34
RM	6.84	11.23	10.76	9.74	6.70	8.26	8.53	6.79	6.29	8.26	8.53	6.79
CF	13.14	11.10	11.54	9.82	11.08	9.54	9.94	8.33	13.74	11.09	10.43	9.19
AC	14.10	11.06	11.53	9.80	16.83	14.22	14.88	12.40	13.92	10.98	12.41	12.30
CT	7.84	10.14	10.43	8.99	3.85	8.56	7.61	6.74	3.99	8.27	7.66	6.68
FS5m	17.64	15.22	15.64	13.49	24.37	23.80	24.69	20.29	30.25	16.79	20.11	27.17
FS10m	29.17	22.96	21.66	18.97	28.63	25.82	24.95	22.77	29.42	25.60	23.41	23.57
FS15m	35.96	35.28	35.69	31.30	39.86	40.27	38.26	34.90	41.62	40.32	49.24	45.57
CW	33.04	32.18	32.55	28.54	26.07	24.67	23.54	22.41	34.36	33.55	32.89	32.23
GW	21.62	21.98	23.64	19.08	32.01	29.56	27.34	21.47	33.92	22.78	25.54	24.43
DB	40.70	41.52	41.99	36.82	39.74	38.85	33.41	36.60	32.41	28.22	27.89	27.56

on both sides of a stream to remove sediment and contaminants from surface runoff (USDA-NRCS, 2016). As shown in Table 4, the efficiency of filter strips in reducing pollutant loads decreased in the future. For example, a FS5m had mean removal rates of 15.22%, 15.64%, and 13.49% for sediment load in the three future periods, but a rate of 17.64% under baseline climate. However, when the width was increased, filter strip efficiencies in the future approached to that of the baseline case. For example, a FS15m had mean removal rates of 35.28%, 35.69%, and 31.30% for sediment load in the three periods, compared to a rate of 35.96% in the baseline climate, and the decrease in efficiencies for TN and TP loads was negligible. The efficiency of filter strips decreased as the number of rainfall and runoff events increased; this result was supported by previous studies (Jayakody et al., 2014; Magette et al., 1989). GWs are channels constructed with covering vegetation to slow water velocity and reduce gully erosion (USDA-NRCS, 2016). According to Table 4, although GWs were effective in reducing sediment and nutrient losses, their efficiency decreased with higher rainfall intensity under future climate change, with decreases of 5.89% and 9.67% respectively in TN and TP removal. This result was consistent with other studies (Wallace et al., 2017). DBs are an important component that increases water self-purification capacity by retaining runoff, sediments, nutrients, and other pollutants (USDA-NRCS, 2016). According to the results in Table 4, DB has an excellent pollutant reduction effect, especially for sediment load, with mean removal rates of 41.52%, 41.99%, and 36.82% in the three future periods respectively. A DB constructed to collect and store storm water, sediment, or debris to preserve ditches, streams, and reservoirs. In this process, nutrients are removed by filtering through soils and vegetation and their microbial processes, with mean removal rates of 38.85%, 33.41%, and 36.60% for TN load and 28.22%, 27.89%, and 27.56% for TP load in the three future periods respectively. Compared to the baseline results, nutrient removal rates were decreased due to short retention time caused by high rainfall intensity and high flow velocity given the future climate in the MRW. Similar results in assessments of other structural BMPs such as CWs and DBs were obtained in other studies (Forsee and Ahmad, 2011; Liu et al., 2017). Filter strips, CWs, GWs, and DBs yielded significant lag times and significant reductions in peak flow, which encouraged infiltration and retention and resulted in substantial reductions in sediment and nutrient loads (Charlesworth, 2010; Liu et al., 2017). However, an increase in precipitation intensity leads to a rapid runoff on slopes, and this process shortens residence time of runoff flowing across these structures, which is not conducive for their effectiveness. Therefore, the increasing frequency of rainfall events, especially extreme rainfall events, in future climate may decrease the efficiency of these BMPs in the MRW. Nevertheless, the structural BMPs produced substantial positive consequences by increasing water, sediment, and nutrient retention in the watershed systems and preventing degradation of terrestrial and aquatic ecosystems.

The SWAT model was set up using the same geographical information, such as DEM, land use, and soil type data, and the same crop management schemes in the baseline and future climates, which was expected to determine similar sources of pollutants and soil disturbance in current and future periods. Non-structural BMPs such as land management and nutrient management practices specialize in controlling pollution loadings by preventing soil erosion, limiting soil-disturbing activities, controlling pollutant sources such as fertilizers and manures, and increasing the efficiency of use of soil nutrients. Therefore, these practices have equivalent efficiency in reducing sediment and nutrient loads under future climate conditions compared to baseline climate. However, decreasing runoff availability for practices relying on runoff management leads to a decrease in their efficiencies. Results indicate that applying CT to all crops in the MRW reduces sediment, TN, and TP loads by 9.85%, 7.64%, and 7.54% on average in future periods. Similar sediment and nutrient load reductions were achieved when RM practices were implemented. Several studies have shown similar results in terms of percent reduction in sediment and nutrient losses due to the application of no-tillage, conservation tillage or residue management at watershed scale (Chen et al., 2016; Dechmi and Skhiri, 2013; Wagena and Easton, 2018). The increase in sediment and nutrient losses was attributed to higher rainfall intensity related to changing climate. Use of a conservation tillage system increased residue cover, which contributed to more infiltration and nutrient transport in the subsurface soil. Reforestation has potentially positive implications for climate change mitigation related to reduced greenhouse gas or carbon emissions (Mbow et al., 2014). It also reduces topsoil erosion, reduces fertilizer input, facilitates nutrient cycling, and enhances soil fertility. In the MRW, CFF25 reduced average annual sediment yields by 11.32%, 11.77%, and 10.02% respectively in the three future periods at subbasin scale, TN loads by 7.68%, 7.29% and 7.46%, and TP loads by 6.70%, 7.11%, and 6.15% with respect to the scenario without any BMPs (CFF25, as shown in Table 4). CFF15 achieved higher reductions due to the larger reforested land area, with mean annual reductions of 14.42%, 15.01%, and 12.76% for sediment yields respectively in the three future periods, 11.76%, 8.17%, and 7.62% for TN loads, and 7.18%, 8.21%, and 6.29% for TP loads (CFF15, as shown in Table 4). These results were supported by other studies (Huang et al., 2017; Mbow et al., 2014). Generally, the efficiency of reforestation practices decreased compared to baseline results because of an increase in overall pollutant loads and a decrease in infiltration and adsorption due to the short residence times of runoff flowing through forestland, which was caused by significantly higher rainfall intensity and flow velocity.

Compared to structural BMPs, CT and conversion to forestland were the sustainable soil/land management systems under future climatic conditions with small adaptations; these results were supported by other studies (Klik and Eitzinger, 2010).

CF and AC are very effective in reducing sheet and rill erosion from water and wind. These two practices can be used to control NPS pollution by reducing transport of sediment, other solids, the contaminants attached to them, and other water-borne contaminants. As shown in Table 4, 10.82% of sediment, 9.27% of TN, and 10.24% of TP reductions were achieved by CF in the future climate, and AC was able to reduce 10.80% of sediment, 13.83% of TN, and 11.90% of TP loads. Compared to baseline climate, the efficiency of these two practices would be decreased under future climates. Extreme heavy rainfall events may decrease effectiveness, with the number of runoff events increasing in the future. This can be explained by turbulent runoff that is not conducive to water infiltration (Rao et al., 2015).

At present, large amounts of urea and manures are being applied to corn, walnuts, and chestnuts in the MRW at annual rates of 200–475 kg/ha based on the field survey. For this reason, nutrient management practices with a reduced application rate of 20% or 30% are recommended. According to Table 4, nutrient management practices had no dominant impact on sediment loss. However, their efficiency was evident in that 12.89%, 13.87%, and 14.85% of TN removal and 14.66%, 14.23%, and 13.80% of TP removal could be achieved by FR20% in the three future periods respectively. Moreover, comparing the results of the three periods, we found that efficiency of TN removal by FR20% was increased in mid-period, whereas efficiency of TP removal was reduced in both mid and late periods. These results were similar to those in other studies (Dechmi and Skhiri, 2013; Jayakody et al., 2014; Rocha et al., 2015).

In this study, with an increase in sediment and nutrient loads under climate variability, non-structural BMPs alone will not be sufficient for watershed management and water quality improvement targets, although they were effective as sustainable management systems under both current and future climate conditions. However, there were uncertainties associated with conservation practice performance. Land cover and soil fertility are compounded by changes in future climate, and therefore BMP efficiency in this study was inconsistent with other studies (Wallace et al., 2017). The effects of climate change on conservation practices are not fully understood despite many efforts to model climate analogs and future climate impacts (Mbow et al., 2014; Yang et al., 2018). The uncertainties of assessing BMP efficiency in reducing sediment and nutrient losses were not accounted for in this study.

3.5. Potential BMP configurations for adaptation to climate change

No single solution or practice meets all future challenges, especially under changing climate. The best strategy is to integrate adaptation options for different situations by combining different practices. This study used a BMP optimization framework to determine potential BMP configurations at sub-basin scale to achieve water-quality improvement targets while minimizing economic cost. Fig. 10(a) shows the costs associated with Pareto-optimality front solutions and the various pollutant loads obtained by implementing these solutions. The TN load was linearly correlated with TP load. The non-structural BMPs were first selected in the evolutionary process because of their low-cost characteristics, after which structural BMPs were included in the BMP combinations as the pollutant removal targets increased due to their high efficiencies in controlling nutrient losses. However, structural BMPs can contribute to high total cost of the optimized results. According to the water-quality improvement targets in the near, middle, and far future periods, three feasible solutions with minimum costs were selected as the BMP combinations to configure within the MRW at

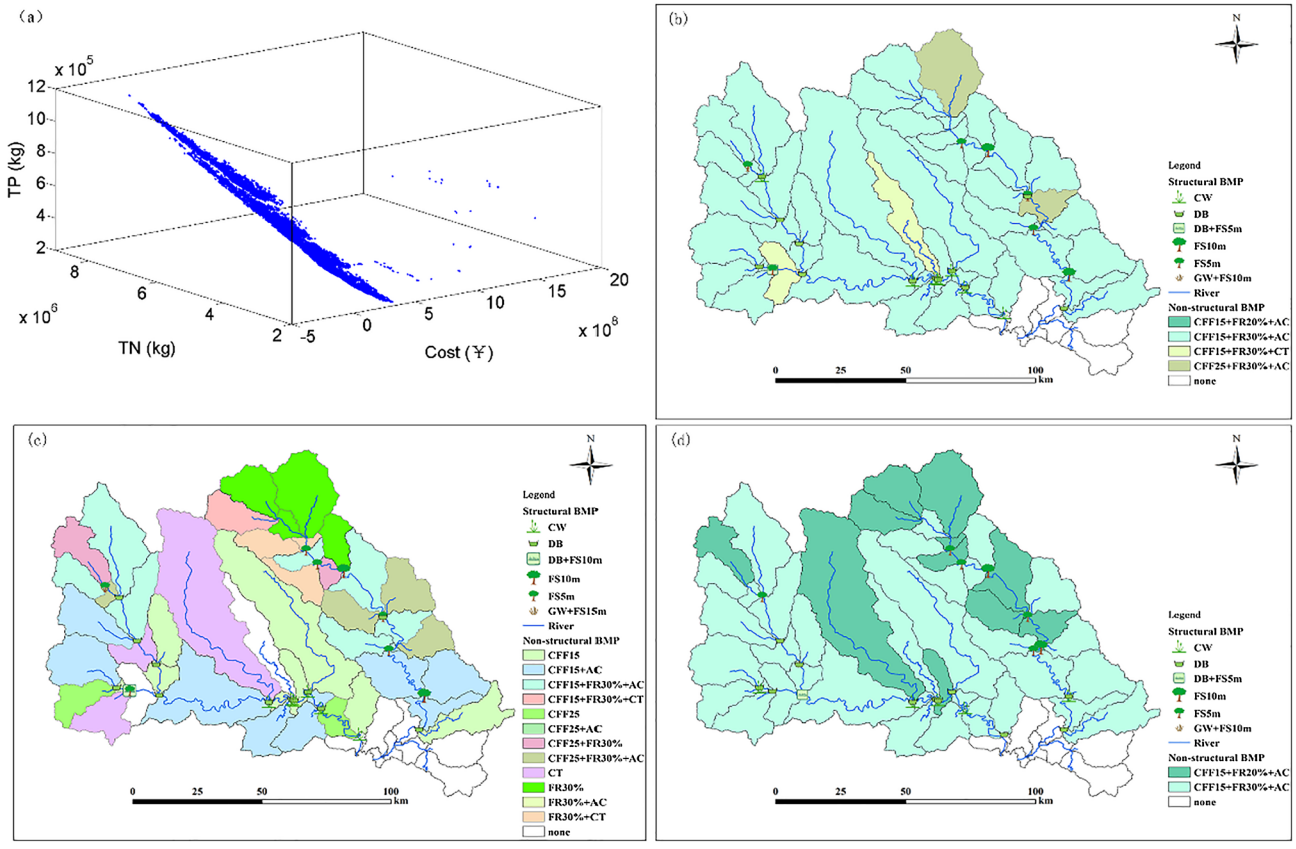

Fig. 10. Pareto-optimality front solutions associated with the cost and various pollutant loads obtained by implementing these solutions (a), and BMP configurations to achieve water-quality targets in the near (2020–2044) (b), middle (c), and far (d) future under climate change.

sub-basin scale (Fig. 10(b), (c), and (d)). Non-structural BMPs were extensively used in all sub-basins, and two or more of them were implemented in critical source areas. As increases in pollutant removal were required, more structural BMPs were involved in the solutions, resulting in higher implementation costs of the BMP combinations. These results indicated that effective watershed management could first be achieved through a combination of non-structural BMPs. To reach further TN and TP reductions, a combination of structural BMPs was suggested for the entire catchment. Almost all sub-basins implemented more than two non-structural BMPs such as RF20% or FR30% and CT, which were always included in each optimal solution, even from an early evolutionary point. Expensive practices, including DB, FS of 5 m and 10 m, and CW, were suggested for inclusion in sub-basins that were identified as critical source areas or priority control areas to achieve control targets for NPS pollution. Generally, the spatial distributions of non-structural BMPs differed in the three future periods, whereas the distributions of structural BMPs were similar in areas identified as the highly polluted sub-basins. This result was supported by other studies (Chen et al., 2016; Qiu et al., 2018).

Due to strict water-quality targets in the middle future, more structural BMPs such as DBs, FS15m, and CWs were configured in highly polluted areas, especially in the Chao River sub-watershed, and many non-structural BMPs were replaced by structural ones that achieved higher removal rates (Fig. 10(c)), which further contributed to higher implementation cost. The implementation cost of BMP schemes for the middle century increased by 13.47% and 7.83% respectively compared to those for the baseline period and the early century.

4. Conclusions

The GCMs for climate variability prediction and the SWAT model for simulations of watershed hydrology and water quality were used to assess the impacts of climate change on hydrology, diffuse pollution, and BMP efficiency in the MRW during 2020–2099. In this study, under RCP 8.5, water balance and water-quality components were impacted by the extent of climate change, which was reflected in significant increases in precipitation amount and temperature in the future. Average change rates of annual runoff for all sub-basins were −30.14%, −22.17%, and −3.97% during the near, middle, and far future periods respectively. The decrease in runoff was driven by a large increase in ET due to significantly increasing temperature rather than by the small increase in precipitation. Sediment, TN, and TP loads at sub-basin scale were increased on average by 12.95%, 7.26% and 9.56% respectively under future climate variability, which was consistent with precipitation trends. These results indicated a strong effect of precipitation on sediment and nutrient losses by the substantial impact of raindrops that directly dislodge and splash soil particles and the contaminants attached to them into runoff and streams. In addition, it was concluded that a unit increase in temperature will lead to 10.11%, 3.77% and 4.51% increases in sediment, TN, and TP loads respectively. Temperature affects sediment yields and nutrient losses by altering soil structure and soil water content and contributing to transformation of various forms of nutrients under different soil temperatures.

With respect to climate change effects on BMP scenarios, the projected changes in future climate resulted in only slight variations in BMP efficiency relative to baseline climate. Implementing non-structural BMPs individually, such as CT, CFF15/CFF25, CF, AC, RM, and FR20%/FR30%, had substantial effects on water quality in surface runoff at the watershed outlet. However, structural BMPs were more effective. DBs were the most effective in reducing sediment loss, and FSs had the greatest effect on reducing nutrient losses. Extreme runoff events caused by high-intensity rainfall in the future could potentially decrease BMP effectiveness.

The simulated efficiencies were used to optimize BMP configurations for adaptation to climate change. More BMPs, especially structural ones, were identified in critical source areas. The number of BMPs implemented increased as the targeted reductions of nutrient loads increased. Filter strips of 15 m were added in the optimized scenarios that achieved high levels of improvement. Almost all sub-basins needed two or more non-structural BMPs to achieve water-quality targets in the three future periods.

This study evaluated the impacts of climate change on NPS pollution and BMP efficiency at sub-basin level. Simulated BMPs were effective in reducing sediment and nutrient losses simultaneously under baseline and future climate scenarios. However, implementation of conservation practices may not be as effective in mitigating the loads of unintended pollutants that could impair water quality. Further research will focus on reducing the loads of these pollutants such as fecal coliform, pesticides, heavy metals, and PAHs.

Declaration of interests

None.

Acknowledgements

This project was supported by the funds from the National Natural Science Foundation of China (No. 51579011) and the fund for Innovative Research Group of the National Natural Science Foundation of China (No. 51721093).

Appendix A. Supplementary data

Supplementary data to this article can be found online at https://doi.org/10.1016/j.jhydrol.2019.03.074.

References

Aguilar, C., Guzman, E., Burguet, M., Jose Polo, M., Taguas, E.V., 2016. Hydrological response of a semiarid olive orchard microcatchment under theoretical climate change scenarios. Soil Sci. 181 (7), 283–292.
Arnold, J.G., et al., 2012a. Soil and Water Assessment Tool Input/Output Documentation, Version 2012. Texas Water Resources Institute, Temple, TX, USA, pp. TR-439..
Arnold, J.G., et al., 2012b. SWAT: model use, calibration, and validation. Trans. ASABE 55 (4), 1491.
Arnold, J.G., Srinivasan, R., Muttiah, R.S., Williams, J.R., 1998. Large area hydrologic modeling and assessment part I: model development. JAWRA J. Am. Water Resour. Assoc. 34 (1), 73–89.
Charlesworth, S.M., 2010. A review of the adaptation and mitigation of global climate change using sustainable drainage in cities. J. Water Clim. Change 1 (3), 165–180.
Chen, L., Wei, G., Shen, Z., 2015. An auto-adaptive optimization approach for targeting nonpoint source pollution control practices. Sci. Rep. 5, 15393.
Chen, L., Wei, G., Shen, Z., 2016. Incorporating water quality responses into the framework of best management practices optimization. J. Hydrol. 541, 1363–1374.
Comino, J.R., et al., 2016. Quantitative comparison of initial soil erosion processes and runoff generation in Spanish and German vineyards. Sci. Total Environ. 565, 1165–1174.
Deb, K., Pratap, A., Agarwal, S., Meyarivan, T., 2002. A fast and elitist multiobjective genetic algorithm: NSGA-II. IEEE Trans. Evol. Comput. 6 (2), 182–197.
Dechmi, F., Skhiri, A., 2013. Evaluation of best management practices under intensive irrigation using SWAT model. Agric. Water Manage. 123 (Suppl. C), 55–64.
Dudula, J., Randhir, T.O., 2016. Modeling the influence of climate change on watershed systems: adaptation through targeted practices. J. Hydrol. 541, 703–713.
Forsee, W.J., Ahmad, S., 2011. Evaluating urban storm-water infrastructure design in response to projected climate change. J. Hydrol. Eng. 16 (11), 865–873.
Gao, J.H., Kirkby, M., Holden, J., 2018. The effect of interactions between rainfall patterns and land-cover change on flood peaks in upland peatlands. J. Hydrol. 567, 546–559.
Geng, R., Zhang, P., Pang, S., Wang, X., Ma, W., 2015. Impact of different climate change scenarios on non-point source pollution losses in Miyun Reservoir watershed. Trans. Chinese Soc. Agric. Eng. 31 (22), 240–249.
Grillakis, M.G., et al., 2016. Initial soil moisture effects on flash flood generation – A comparison between basins of contrasting hydro-climatic conditions. J. Hydrol. 541, 206–217.
Haas, M.B., Guse, B., Fohrer, N., 2017. Assessing the impacts of best management practices on nitrate pollution in an agricultural dominated lowland catchment considering environmental protection versus economic development. J. Environ. Manage. 196, 347–364.
Hashemi, F., Olesen, J.E., Dalgaard, T., Borgesen, C.D., 2016. Review of scenario analyses to reduce agricultural nitrogen and phosphorus loading to the aquatic environment. Sci. Total Environ. 573, 608–626.
Hempel, S., Frieler, K., Warszawski, L., Schewe, J., Piontek, F., 2013. A trend-preserving

bias correction-the ISI-MIP approach. Earth Syst. Dyn. 4 (2), 219–236.
Hijioka, Y., Matsuoka, Y., Nishimoto, H., Masui, T., Kainuma, M., 2008. GlobalL GHG emission scenarios under GHG Concentration Stabilization Targets. J. Global Environ. Eng. 13, 97–108.
Huang, C., et al., 2017. Quantificational effect of reforestation to soil erosion in sub-tropical monsoon regions with acid red soil by sediment fingerprinting. Environ. Earth Sci. 76 (1).
Jayakody, P., Parajuli, P.B., Cathcart, T.P., 2014. Impacts of climate variability on water quality with best management practices in sub-tropical climate of USA. Hydrol. Process. 28 (23), 5776–5790.
Kendall, M.G., 1975. Rank Correlation Methods. Charles Griffin, London, pp. 35.
Kiedrzynska, E., Kiedrzynski, M., Zalewski, M., 2015. Sustainable floodplain management for flood prevention and water quality improvement. Nat. Hazards 76 (2), 955–977.
Kim, S.B., Shin, H.J., Park, M., Kim, S.J., 2015. Assessment of future climate change impacts on snowmelt and stream water quality for a mountainous high-elevation watershed using SWAT. Paddy Water Environ. 13 (4), 557–569.
Klik, A., Eitzinger, J., 2010. Impact of climate change on soil erosion and the efficiency of soil conservation practices in Austria. J. Agric. Sci. 148 (5), 529–541.
Leng, G., Tang, Q., 2014. Modeling the impacts of future climate change on irrigation over China: sensitivity to adjusted projections. J. Hydrometeorol. 15 (5), 2085–2103.
Liu, Y., Engel, B.A., Collingsworth, P.D., Pijanowski, B.C., 2017. Optimal implementation of green infrastructure practices to minimize influences of land use change and climate change on hydrology and water quality: case study in Spy Run Creek watershed, Indiana. Sci. Total Environ. 601, 1400–1411.
Lv, M., et al., 2016. Reservoir operation with feedback in a coupled land surface and hydrologic model: a case study of the huai river Basin, China. JAWRA J. Am. Water Resour. Assoc. 52 (1), 168–183.
Ma, H., Yang, D., Tan, S.K., Gao, B., Hu, Q., 2010. Impact of climate variability and human activity on streamflow decrease in the Miyun Reservoir catchment. J. Hydrol. 389 (3), 317–324.
Magette, W.L., Brinsfield, R.B., Palmer, R.E., Wood, J.D., 1989. Nutrient and sediment removal by vegetated filter strips. Trans. ASAE 32 (2), 663–0667.
Mann, H.B., 1945. Nonparametric tests against trend. Econometrica 13 (3), 245–259.
Mbow, C., Smith, P., Skole, D., Duguma, L., Bustamante, M., 2014. Achieving mitigation and adaptation to climate change through sustainable agroforestry practices in Africa. Curr. Opin. Environ. Sustain. 6, 8–14.
Milly, P.C.D., Dunne, K.A., 2016. Potential evapotranspiration and continental drying. Nat. Clim. Change 6, 946.
Pan, Z., Zhang, Y., Liu, X., Gao, Z., 2016. Current and future precipitation extremes over Mississippi and Yangtze River basins as simulated in CMIP5 models. J. Earth Sci. 27 (1), 22–36.
Panagopoulos, Y., et al., 2015. Impacts of climate change on hydrology, water quality and crop productivity in the Ohio-Tennessee River Basin. Int. J. Agric. Biol. Eng. 8 (3), 36–53.
Qiu, J., Shen, Z., Huang, M., Zhang, X., 2018. Exploring effective best management practices in the Miyun Reservoir Watershed, China. Ecol. Eng. 123, 30–42.
Rao, B.K., Kurothe, R.S., Mishra, P.K., Kumar, G., Pande, V.C., 2015. Climate change impact on design and costing of soil and water conservation structures in watersheds. Curr. Sci. 108 (5), 960–966.
Renkenberger, J., et al., 2017. Effectiveness of best management practices with changing climate in a Maryland watershed. Trans. ASABE 60 (3), 769–782.
Riahi, K., Gruebler, A., Nakicenovic, N., 2007. Scenarios of long-term socio-economic and environmental development under climate stabilization. Technol. For. Soc. Change. 74 (7), 887–935.
Rocha, J., Roebeling, P., Rial-Rivas, M.E., 2015. Assessing the impacts of sustainable agricultural practices for water quality improvements in the Vouga catchment (Portugal) using the SWAT model. Sci. Total Environ. 536, 48–58.
Saraswat, C., Kumar, P., Mishra, B.K., 2016. Assessment of stormwater runoff management practices and governance under climate change and urbanization: An analysis of Bangkok, Hanoi and Tokyo. Environ. Sci. Policy 64, 101–117.
Saxton, K.E., Rawls, W.J., 2006. Soil water characteristic estimates by texture and organic matter for hydrologic solutions. Soil Sci. Soc. Am. J. 70 (5), 1569–1578.
Smith, S.J., Wigley, T.M.L., 2006. Multi-gas forcing stabilization with minicam. Energy J. 27, 373–391.
Sofia, G., Ragazzi, F., Giandon, P., Dalla Fontana, G., Tarolli, P., 2019. On the linkage between runoff generation, land drainage, soil properties, and temporal patterns of precipitation in agricultural floodplains. Adv. Water Resour. 124, 120–138.
Sun, N., et al., 2016. A spatially distributed model for assessment of the effects of changing land use and climate on urban stream quality. Hydrol. Process. 30 (25), 4779–4798.
USDA-NRCS, 2016. National Conservation Practices Standards. https://www.nrcs.usda.gov/wps/portal/nrcs/detailfull/national/technical/cp/ncps/?cid=nrcs143_026849.
Valcu-Lisman, A.M., Gassman, P.W., Arritt, R., Campbell, T., Herzmann, D.E., 2017. Cost-effectiveness of reverse auctions for watershed nutrient reductions in the presence of climate variability: An empirical approach for the Boone River watershed. J. Soil Water Conserv. 72 (3), 280–295.
van Vuuren, D.P., et al., 2007. Stabilizing greenhouse gas concentrations at low levels: an assessment of reduction strategies and costs. Clim. Change 81 (2), 119–159.
van Vuuren, D.P., et al., 2011. The representative concentration pathways: an overview. Clim. Change 109 (1), 5.
Volk, M., Bosch, D., Nangia, V., Narasimhan, B., 2017. SWAT: Agricultural water and nonpoint source pollution management at a watershed scale—Part II. Elsevier.
Wagena, M.B., Easton, Z.M., 2018. Agricultural conservation practices can help mitigate the impact of climate change. Sci. Total Environ. 635, 132–143.
Waidler, D., et al., 2011. Conservation Practice Modeling Guide for SWAT and APEX. Texas Water Resources Institute.
Wallace, C.W., Flanagan, D.C., Engel, B.A., 2017. Quantifying the effects of conservation practice implementation on predicted runoff and chemical losses under climate change. Agric. Water Manage. 186, 51–65.
Yang, X., et al., 2018. Impacts of climate change on TN load and its control in a River Basin with complex pollution sources. Sci. Total Environ. 615, 1155–1163.
Yasarer, L.M.W., et al., 2017. Climate change impacts on runoff, sediment, and nutrient loads in an agricultural watershed in the lower Mississippi River Basin. Appl. Eng. Agric. 33 (3), 379–392.
Zessner, M., et al., 2017. A novel integrated modelling framework to assess the impacts of climate and socio-economic drivers on land use and water quality. Sci. Total Environ. 579, 1137–1151.
Zheng, J., et al., 2016. Impacts of Land Use Change and Climate Variations on Annual Inflow into the Miyun Reservoir. Hydrology and Earth System Sciences, Beijing, China.